Modelling Particulate Removal in Tubular Wet Electrostatic Precipitators Using a Modified Drift Flux Model

S. Ramechecandane[1*], C. Beghein[2]
[1] Senior Software Developer, WindSim AS, Tonsberg 3115, Norway
[2] Associate Professor, Pole Sciences et Technologie,
Universite de La Rochelle, La Rochelle 17000, France

ABSTRACT
Tubular electrostatic precipitators (ESP) have been used in a number of chemical processing industries. The tubular ESPs have many advantages over conventional plate-plate and wire-plate ESPs. The present study is concerned with the numerical modeling of particulate removal in a tubular wet single-stage electrostatic precipitator (wESP). The geometric parameters of a model wESP and the corresponding inlet gas velocities for the wESP are chosen from available experimental data. In addition to the RNG $k - \varepsilon$ model for the mean turbulent flow field inside the wESP, the Poisson equation for the electric field, the charge continuity equation and the concentration equation are solved sequentially to obtain a full-fledged solution to the problem under investigation. The proposed drift flux model is implemented in the opensource CFD code OpenFOAM®. The paper discusses the influence of the number of charges acquired by the particles and the corresponding inlet gas velocities on particle concentration distribution within the wESP. Two representative cases with monodispersed particles of 1 μm and 10 μm diameter are considered for the numerical analysis. It is seen from the present analysis that the number of units of charge on particles, the particle size and the inlet gas velocities play a vital role in determining the efficiency of electrostatic precipitation.

Keywords: tubular electrostatic precipitator, electric field, drift flux model, particle removal, computational fluid dynamics

ABBREVIATIONS

DPM	Diesel Particulate Matter
ESP	Electrostatic Precipitator
wESP	Wet Electrostatic Precipitator

1. INTRODUCTION

The man made or anthropogenic sources contribute to the majority of the pollutant concentration near the earth's surface. The majority of these hazardous aerosols are concentrated in the lower 1–2 km of the troposphere, where most of the global population lives. The flue gases are

* Corresponding author: Email id:ramesh@windsim.com
Telephone: +47 95446874

carcinogenic and may lead to acute heart diseases. New energy policies and global awareness towards climatic change and ozone depletion has resulted in more stringent emission standards that are imposed on dust control devices. Increased per capita power consumption in well developed nations and the ever growing automobile sector plays an undeniable role in contaminating the atmosphere. The flue gases emanating from the fossil fuel powered power plants and process/chemical industries contain a number of carcinogenic contaminants that are disposed continuously into the atmosphere. A means of containing these pollutants and dust particles present in flue/stack gases is to subject them to electrostatic precipitation.

Conventional electrostatic precipitators are electrostatic devices known for cleaning flue gases released from power plants and process industries by removing dust and other hazardous contaminants that pollute the atmosphere. These devices exploit the electrical forces to facilitate the removal of particulate pollutants. In the past few decades, lot of attention has been bestowed on ESPs and various designs were proposed with an objective of increasing cleaning efficiency. A detailed review of literature shows that in the last twenty years the total number of papers published in sciencedirect (www.sciencedirect.com) is 431. This marks a two-fold rise in the number of research papers published in this particular area of research. Figure 1 shows the number of research papers published on ESPs since 1991. Majority of these research works on ESPs, were mainly focused on parallel–plate ESPs rather than tubular ESPs. The amount of attention bestowed on tubular ESPs is quite meager. Of the 431 papers on ESPs it is seen that hardly 4 papers discuss about tubular ESPs [1–4]. The only study to quantitatively compare the single-stage and two-stage tubular ESPs was by Surati et al. [1].

According to Surati et al. [1] the plate type ESPs are inadequate in applications where very high loading and/or high particulate content are involved. Tubular design with wider spacing and higher voltages incorporates the best features of both the single-stage and two-stage ESPs. These units are found in molybdenum roasting, zirconium calcining, ammonia scrubbing of oxides of sulphur, meat broiling, foundry exhaust etc. The concept of wet electrostatic precipitation has evolved quite recently and is quite promising in terms of containing sub micron sized particles. In a wESP the collecting electrode is smeared with oil or water to have higher capture efficiency [2].

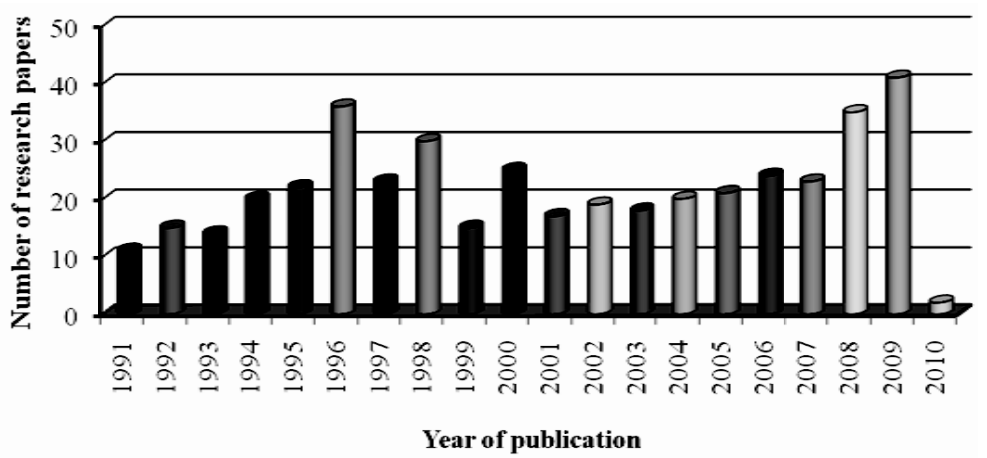

Figure 1: Number of papers on electrostatic precipitators published in the last twenty years (Prior to 1990 the total number of papers were 202 - courtesy www.sciencedirect.com)

The objective of the present study is to propose a modified drift flux model to simulate the dispersion and deposition of contaminants in a tubular wESP. A model wet electrostatic precipitator (wESP) of Saiyasitpanich [2] is considered for the present numerical study. A parametric study is conducted for different particle sizes and for different gas inlet velocities. The effect of the number charges on the particles is also explored using the proposed model.

2. MATHEMATICAL FORMULATION

The mathematical model developed for the present investigation on wESP is built on some basic assumptions:

(i) The particles are assumed to be spherical in shape. The liquid droplets are usually spherical in shape whereas the solid particles can have irregular shapes that can be approximated as spheres based on previous studies.

(ii) The interactions between particles like collisions and coagulation/ agglomeration can be neglected. As the particles agglomerate the size of the particles increase and hence may get precipitated faster than smaller particles. In the present investigation a monodispersed assumption is made ignoring the effect of coagulation/ agglomeration.

(iii) There exists no bounce-off or re-entrainment of the particles once they reach the collecting wall. i.e., the collecting walls are assumed to be perfect absorbers. This is a valid assumption as in the wESP, the surface of the collecting electrode is smeared with oil or other liquids.

(iv) Saturation charging can be achieved in 0.01 s or less for most industrial applications encountered. Hence the particles can be assumed to be pre-charged even before entering the wESP [5]. This assumption leads to a reduction in the computational complexity.

2.1. FLOW FIELD

Using Reynolds averaging, the continuity and momentum equations in Cartesian coordinates turn out to be

$$\frac{\partial}{\partial x_i}(\rho\overline{u}_\iota) = 0 \tag{1}$$

$$\frac{\partial}{\partial t}(\rho\overline{u}_\iota) + \frac{\partial}{\partial x_j}\left(\rho\overline{u}_\iota\overline{u}_J\right) = -\frac{\partial\bar{p}}{\partial x_i} + \frac{\partial}{\partial x_j}\left[\mu_t\left(\frac{\partial\overline{u}_\iota}{\partial x_j} + \frac{\partial\overline{u}_j}{\partial x_i}\right)\right] + \frac{\partial}{\partial x_j}\left(-\rho\overline{u_\iota' u_j'}\right) \tag{2}$$

The Reynolds stresses $\rho\overline{u_i' u_j'}$ in the eqn. 2 must be modeled in order to close the equation. A common method employs the Boussinesq hypothesis to relate the Reynolds stresses to the mean velocity gradients

$$-\rho\overline{u_\iota' u_j'} = \mu_t\left(\frac{\partial\overline{u}_\iota}{\partial x_j} + \frac{\partial\overline{u}_j}{\partial x_i}\right) - \frac{2}{3}\rho k\delta_{ij} \tag{3}$$

The advantage of this approach is the relatively low computational cost associated with the computation of the turbulent viscosity (μ_t). In the case of the RNG $k-\varepsilon$ model, two additional

transport equations (for the turbulent kinetic energy k, and the turbulent dissipation rate ε) are solved, and μ_t is computed as a function of k and ε.

$$\frac{\partial(\rho k)}{\partial t} + \frac{\partial}{\partial x_j}\left(\rho k \overline{u_j}\right) = \frac{\partial}{\partial x_j}\left((\mu + \alpha_k \mu_t)\frac{\partial k}{\partial x_j}\right) + G_k - \rho\varepsilon \tag{4}$$

$$\frac{\partial(\rho \varepsilon)}{\partial t} + \frac{\partial}{\partial x_j}\left(\rho \varepsilon \overline{u_j}\right) = \frac{\partial}{\partial x_j}\left((\mu + \alpha_\varepsilon \mu_t)\frac{\partial \varepsilon}{\partial x_j}\right) + C_{1\varepsilon} G_k \frac{\varepsilon}{k} - C_{2\varepsilon}\rho\frac{\varepsilon^2}{k} - R_\varepsilon \tag{5}$$

$$\mu_t = \rho C_\mu \frac{k^2}{\varepsilon} \tag{6}$$

The major parameters that differentiate RNG $k - \varepsilon$ model from the standard $k - \varepsilon$ model are the constants involved in the equations (4) and (5) and the term R_ε that is present in the right hand side of eqn (5), and is given by.

$$R_\varepsilon = \frac{C_\mu \rho \eta^3 \left(1 - \frac{\eta}{\eta_0}\right)}{1 + \beta\eta^3}\frac{\varepsilon^2}{k} \tag{7}$$

Where,

$$\eta = \frac{k}{\varepsilon}\left[\left(\frac{\partial \overline{u_i}}{\partial x_j} + \frac{\partial \overline{u_j}}{\partial x_i}\right)\frac{\partial \overline{u_i}}{\partial x_j}\right]^{1/2}$$

The values of constants involved in eqns (4), (5) and (6) are given in Table. 1

Table 1: Constants involved in the RNG k-ε model

C_μ	C_{1e}	$C_{2\varepsilon}$	α_k	α_e	η_0	β
0.0845	1.42	1.68	0.7194	1.39	4.38	0.012

The term G_k representing the production of turbulent kinetic energy is modeled as

$$G_k = -\rho\overline{u'_i u'_j}\frac{\partial \overline{u_i}}{\partial x_j} \tag{8}$$

In order to obtain the flow field of a wESP the momentum eqn (2) should incorporate a source term to account for the effect of electric field, the modified momentum equation that has to be solved is

$$\frac{\partial(\rho\overline{u}_i)}{\partial t} + \frac{\partial}{\partial x_j}\left(\rho\overline{u}_i\overline{u}_j\right) = -\frac{\partial\bar{p}}{\partial x_i} + \frac{\partial}{\partial x_j}\left[\mu\left(\frac{\partial\overline{u}_i}{\partial x_j} + \frac{\partial\overline{u}_j}{\partial x_i}\right)\right] + \frac{\partial}{\partial x_j}\left(-\rho\overline{u_i'u_j'}\right) + \rho_{el,I}E_j \quad (9)$$

The continuity eqn (1) and the modified momentum equation (9) with the RNG $k - \varepsilon$ model (Eqns. 4–8) for the mean turbulent flow field are solved using an opensource CFD code – OpenFOAM – version 1.5.

2.2. SIMULATION OF ELECTRIC FIELD

In the present study a numerical solution of the electric field is obtained by solving the Poisson equation and the equation for charge continuity.

The electric field is given as,

$$\vec{E} = -\overrightarrow{grad}\varphi \quad (10)$$

Where φ is the applied voltage, and is obtained by solving the Poisson equation

$$\Delta\varphi = -\frac{\rho_{el,I} + \rho_{el,P}}{\varepsilon_0} \quad (11)$$

Where, $\varepsilon_0 = 8.8593 \times 10^{-12}\ A\ s\ V^{-1}m^{-1}$ is the dielectric permittivity of air; $\rho_{el,I}$ and $\rho_{el,P}$ are the ionic and particulate space charge respectively. The continuity equation for the ionic space charge neglecting the effects of mean fluid flow convection and diffusion is given by [8]

$$\mathrm{div}\overrightarrow{Jel,I} = 0 \quad (12)$$

$$\overrightarrow{Jel,I} = \rho_{el,I}b_I\vec{E}. \quad (13)$$

Where, $b_I = 23 \times 10^{-4}\ m^2\ V^{-1}\ s^{-1}$ is the ionic mobility for a negative corona discharge [8,9]

In the present investigation, the particles are assumed to be electrically charged even before entering the electric field and hence acquire an electrical migration velocity purely based on the electric field and the number of charges already on the particles. Eqs. (11) and (12) form a set of partial differential equations that are to be solved for computing the

Table 2: Boundary conditions for the single-stage tubular wESP

	x–velocity (m/s)	**y–velocity (m/s)**	**Electric potential (kV)**	**Ion charge density**	**Particle fate**
Inlet	1.0	0	$\frac{\partial\varphi}{\partial x} = 0$	$\frac{\partial\rho_{el,i}}{\partial x} = 0$	escape
Outlet	constant static pressure	$\frac{\partial p}{\partial x} = 0$	$\frac{\partial\varphi}{\partial x} = 0$	$\frac{\partial\rho_{el,i}}{\partial x} = 0$	escape
Collecting electrode	no slip	no slip	$\phi = 0$	$\frac{\partial\rho_{el,i}}{\partial y} = 0$	trap
Discharge Wire	no slip	no slip	70	0.0001	reflect

potential field and thereby, the electric field with the charge density distribution for a wESP (Table 2).

The number of units of charge on a particle needs to be calculated by taking into account the various charging mechanisms like the static electrification, tribo-electrification, Boltzmann charge distribution, the diffusion charging and the field charging mechanisms. One can decide from existing literature [9] that the diffusion and field charging mechanism is more apt for micro-sized particles.

The effect of field charging is quite significant for particles that are larger than 1 μm in size and increases with the square of the particle size. After sufficient time at a given charging condition, the maximum saturation number of charges "n_{field}", acquired by the particles is given by,

$$n_{field} = \left(\frac{3\varepsilon_0}{\varepsilon_0 + 2}\right)\left(\frac{E d_p^{\,2}}{4e}\right) \tag{14}$$

Where, E is the magnitude of the electric field, $\varepsilon_0 = 8.859 \times 10^{-12}\ A\ s\ V^{-1}\ m^{-1}$ is the dielectric permittivity, $e = 1.63 \times 10^{-19}$ C is the electronic unit charge.

For particles less than 1 μm in size, diffusion charging is the main charging mechanism.

The approximate number of charges acquired by a particle of diameter d_p is given by,

$$n_{diffusion} = \left(\frac{d_p k_\beta T}{2e^2}\right)\ln\left(1 + \frac{\pi d_p \bar{c}_1 e^2 N_i t}{2k_\beta T}\right) \tag{15}$$

Where, $k_\beta = 1.38 \times 10^{-16}$ erg K^{-1} is the Boltzmann constant, T is the temperature of the gas and equals to 288 K, $e = 1.63 \times 10^{-19}$ C is the electronic unit charge, t stands for time, $\bar{c}_1 = 2.4 \times 10^{24}$ cm s^{-1} is the mean thermal speed of ions; N_i is the ions concentration.

The total number of charges that a single particle can acquire by both field charging and diffusion charging mechanisms is given by,

$$q_p = (n_{field} + n_{diffusion})e \tag{16}$$

2.3 MODIFIED DRIFT FLUX MODEL

The modified drift flux model to account for the drift flux caused by the inhomogeneous electric field is given by [8]

$$\frac{\partial \overline{C^\alpha}}{\partial t} + \frac{\partial}{\partial x_j}\left(\left(\overline{u_j} + \mu_P E_j\right)\overline{C^\alpha}\right) = \frac{\partial}{\partial x_j}\left(\left(D^\alpha + \frac{\nu_t}{Sc_t^\alpha}\right)\frac{\partial \overline{C^\alpha}}{\partial x_j}\right) \tag{17}$$

Where, μ_P the dielectric particle mobility or the electrical mobility of a particle is given by

$$\mu_P = \frac{q_p C_c}{3\pi\mu d_p} \tag{18}$$

The modified drift flux model given by Eq. (17) is solved to obtain the normalized

concentration for various particle sizes/diameters. In equation 17 the term $\mu_P E_j$ is normally referred to as the electrical migration velocity given by equating the Coulomb force to the Stokes drag. The electrical migration velocity w_e is given by,

$$w_e = \frac{q_p C_c E}{3\pi\mu d_p} \tag{19}$$

The numerical analysis employed to solve the present problem is based on the finite volume formulation with the central difference scheme for the diffusion terms and the quadratic upwind weighted scheme for the convection terms to eliminate the false diffusion. Euler implicit scheme is employed for the temporal discretization.

2.4 DEUTSCH-ANDERSON EQUATION

To qualitatively compare the results obtained using the proposed drift flux model the predicted removal efficiencies for various operating conditions are compared with the less accurate Deutsch-Anderson equation. The exponential Deutsch-Anderson equation has been in wide use in the design of single-stage precipitators and is given as

$$\eta = 1 - \exp(-Aw / V) \tag{20}$$

Where, A is the collecting electrode area, V the volumetric flow rate and w the drift velocity.

For a single stage tubular electrostatic precipitators,

$$\frac{A}{V} = \frac{2\pi RL}{\pi R^2 v} = \frac{2L}{Rv} \tag{21}$$

where, v is the inlet gas velovity

Hence, the Deutsch-Anderson equation for tubular single stage electrostatic precipitators is given by

$$\eta = 1 - \exp\left(-\frac{2Lw}{Rv}\right) \tag{22}$$

Velocity through the precipitator is the only flow parameter involved in Deutsch-Anderson equation. The Deutsch-Anderson equation assumes plug flow velocity distribution. The precision of estimates from the Deutsch-Anderson equation is usually ± 50% [3].

2.5. DISCRETIZATION

The space domain is discretized into computational mesh on which the partial differential equations are subsequently discretized. The discretization of the space requires the subdivision of the domain into a number of cells, or control volumes. The cells are contiguous, i.e., they do not overlap one another and completely fill the domain. Dependent variables and other properties are stored at the cell centroid (colocated vertices). Fig. 2 shows two control volumes with P and N as centroids. The face f is the internal face that lies between the two control volumes. The various terms in the governing equations those were discussed in the section on mathematical formulation are integrated and linearized as follows:

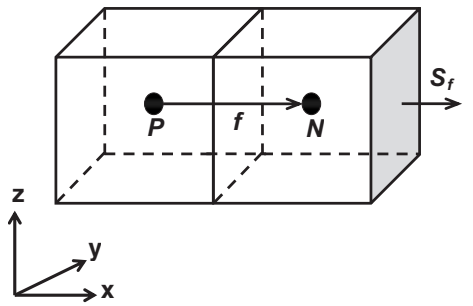

Figure 2: parameters in finite volume discretization

The Laplacian term is integrated over a control volume and integrated as follows:

$$\int_V \nabla \cdot (\Gamma \nabla \phi) dV = \int_S dS \cdot (\Gamma \nabla \phi) = \sum_f \Gamma_f S_f \cdot (\nabla \phi)_f \tag{23}$$

The face gradient discretization is implicit when the length vector d between the center of the cells of interest P and the neighboring cell N is orthogonal to the face plane, i.e., parallel to S_f.

$$S_f . (\nabla \phi)_f = |S_f| \frac{\phi_N - \phi_P}{|d|} \tag{24}$$

The convection term is integrated over a control volume and linearized as follows:

$$\int_V \nabla \cdot (\rho U \phi) dV = \int_S dS \cdot (\rho U \phi) = \sum_f S_f . (\rho U)_f \phi_f = \sum_f F \phi_f \tag{25}$$

The face field ϕ_f is evaluated using a quadratic upwind scheme.

The temporal discretization is using an Euler implicit scheme that is first order accurate in time:

$$\frac{\partial}{\partial t} \int_V \rho \phi dV = \frac{(\rho_P \phi_P V)^n - (\rho_P \phi_P V)^o}{\Delta t} \tag{26}$$

Where *n* denotes the new values and *o* stands for the old values.

4. RESULTS AND DISCUSSION

4.1. COMPUTATIONAL DOMAIN

The present investigation is restricted to wet tubular single stage ESP (wESP) that finds its application in the removal of diesel particulate matter (DPM). The geometry considered for the present numerical analysis is the same as the model precipitator of Saiyasitpanich [2]. The wESP has a large grounded cylinder known as the collecting electrode and, coaxial with it a high potential wire called the discharge electrode. Though the overall length of the wESP

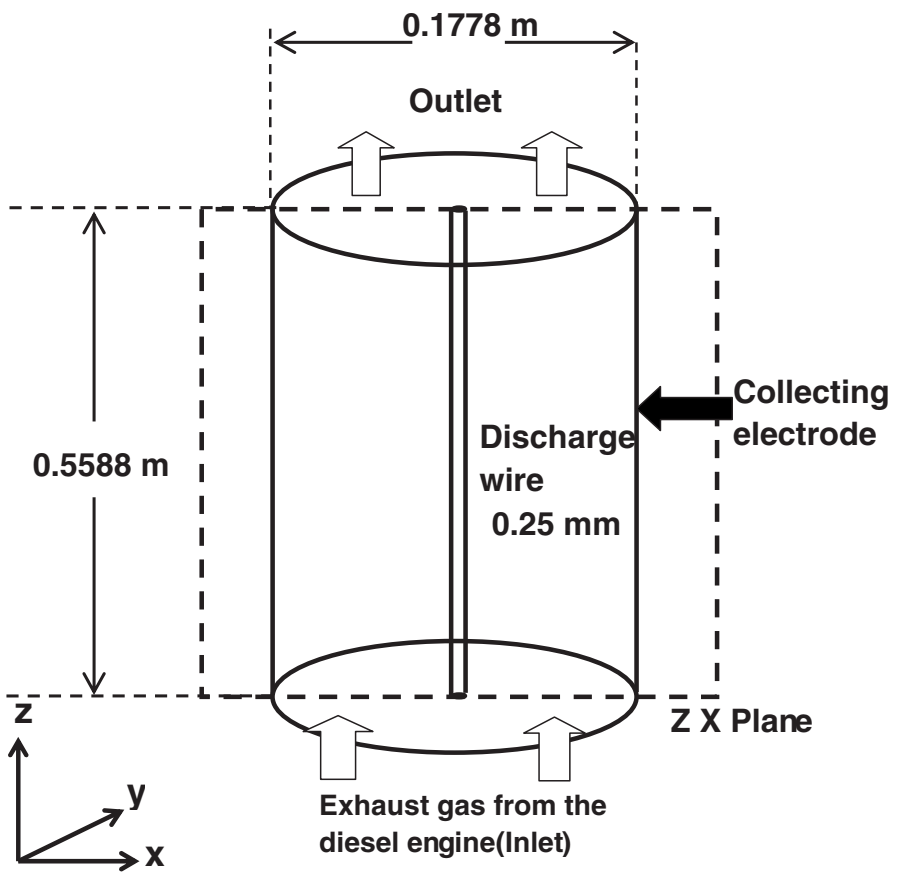

Figure 3: Schematic of the geometry considered for investigation (figure not to scale)

is 0.914 m the effective collection length is 0.5588 m. The diameter of the collecting electrode is 0.1788 m and the discharge electrode is 0.25 mm in diameter. A schematic of the geometry considered for the present investigation is shown in Fig. 3. The discharge electrode is supplied with an electric potential of 70 kV. As the geometry is axi-symmetric just one quarter of the whole domain is considered for the numerical investigation. A block structured mesh is generated for the $1/4^{th}$ of the complete geometry and is presented in Fig. 4. The grid generated for the present investigation comprises of 40000 hexahedral elements. A grid independence study has been carried out using 40000 cells and 320000 cells and it is seen that the variation in the solution obtained for the flow field is less than 1%. It is also seen that a grid size of 40000 elements is sufficiently fine enough to ensure a y^+ value less than 1 at the walls. For the present analysis inlet gas velocities of 1.4, 4.5 and 5.6 m/s are considered (similar to the work of Saiyasitpanich [2]) with a turbulent intensity of 3%.

4.2. ELECTRIC FIELD VALIDATION

To validate the electric field obtained by the numerical simulation, the computational results are compared with the often-quoted experimental works of Penney and Matick [10] and the numerical studies of Lami et al. [11]. The electric potential and the charge density distribution are computed for the precipitator geometry of Penney and Matick with the wire diameter of 2

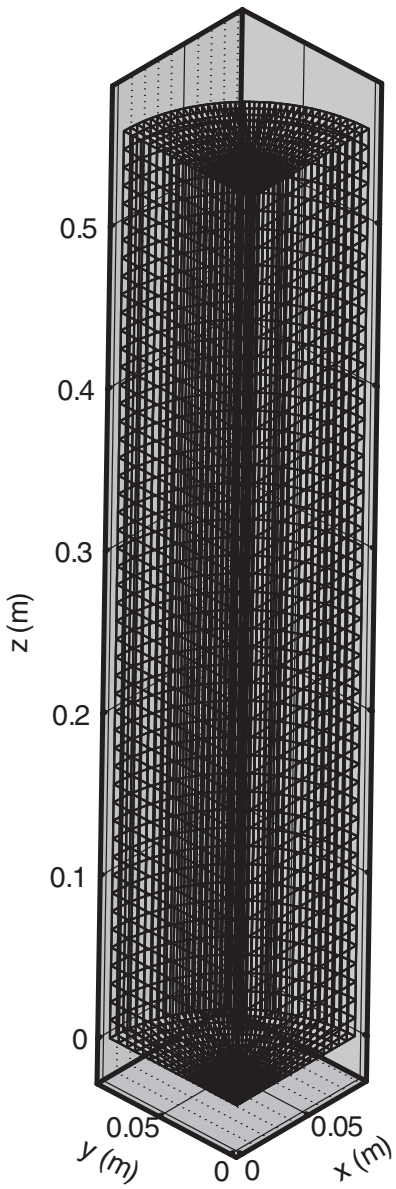

Figure 4: Grid generated for the computational domain (1/4 of the complete domain is considered owing to symmetry)

mm and an applied voltage of 46.2 kV at the wire. The schematic of the geometry considered for the present investigation is shown in Fig. 5. Owing to symmetry just one fourth of the geometry is considered for the numerical analysis. The computational domain considered for the numerical analysis consists of hexahedral elements and the grid is sufficiently fine enough to ensure a y^+ value less than 1. A part of the computational mesh considered for the analysis is shown in Fig. 6. The electric potential distribution along a line from the wire electrode to the collector plate is plotted in Fig. 7 and the corresponding charge density distribution from the present numerical simulation is shown in Fig. 8. The numerical results obtained using the

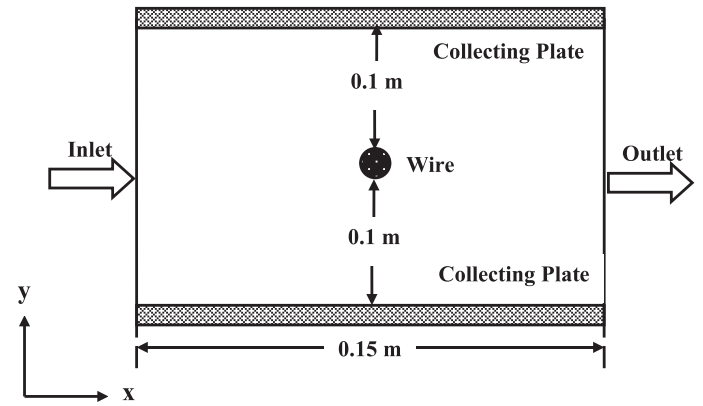

Figure 5: Model configuration for the wire-plate electrostatic precipitator (not to scale)

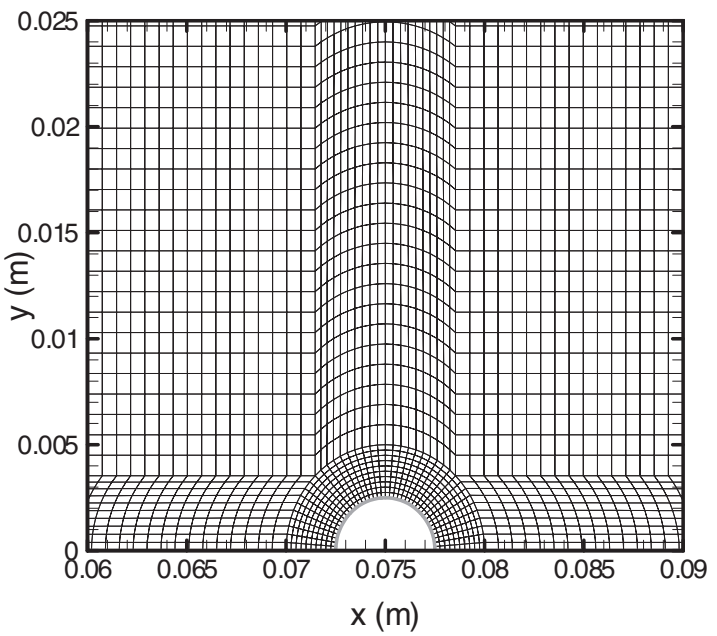

Figure 6: Computational mesh near the wire

present numerical simulation for the bench mark case of Penney and Matick show a good agreement with the experimental data. The obtained results are also compared with the numerical studies of Lami et al. [11] and are presented in Figs. 9 and 10. The computational mesh considered by Lami et al. is coarser as compared to the mesh adapted for the present investigation. Nevertheless, the results obtained show good agreement with the numerical results published by Lami et al.

4.3. INFLUENCE OF THE PARTICLE SIZE ON REMOVAL EFFICIENCY OF WESP

Fig. 11 presents the contours of the flow field, electric field and concentration field for an inlet gas velocity of 1.4 m/s and a particle size of 1 μm. The results obtained for one quarter

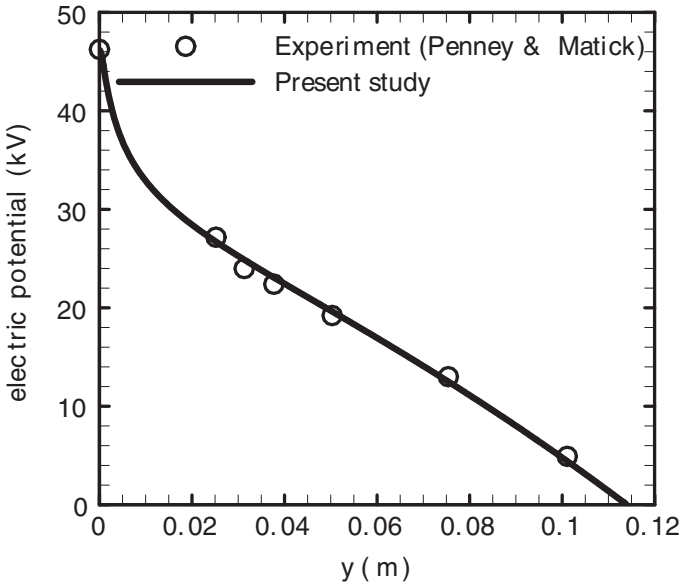

Figure 7: Comparison of measured and predicted electric potentials for the test case (Penney and Matick [10])

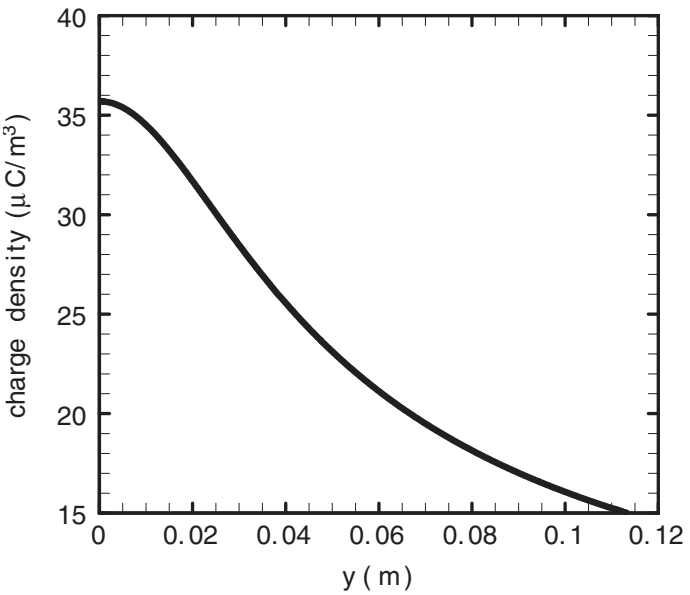

Figure 8: Ionic space charge density distribution for the test case (Penney and Matick [10])

of the computational domain is mirrored to get the results presented for one half of the wESP in Fig. 11. The contours for other inlet gas velocities (i.e., 4.5 and 5.6 m/s) are not presented for the sake of brevity. As the applied voltage is the same for all the three inlet gas velocities, the contours of electric potential and charge density remain unchanged. However, as

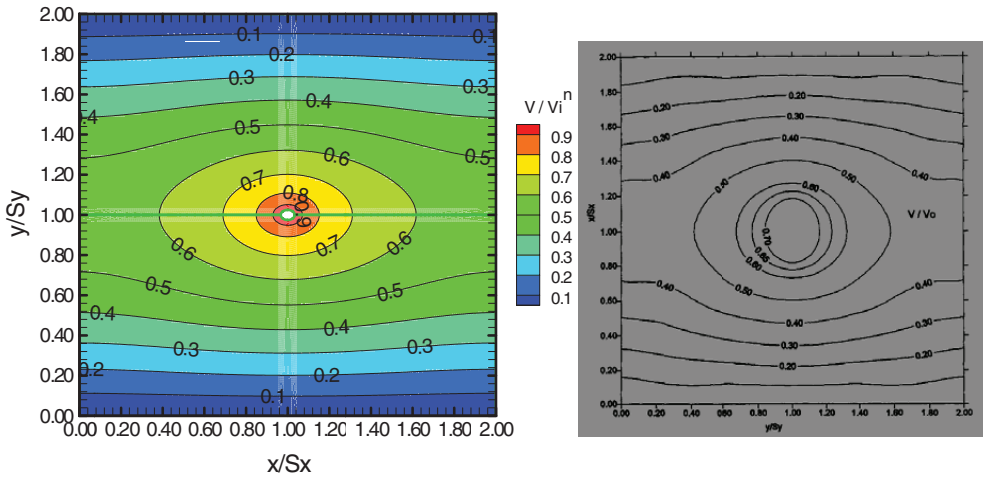

(a) Normalized electric potential – Present study

(b) Normalized electric potential – Lami et al

Figure 9: Normalized electric potential distribution – electric potential is normalized using the applied electric potential at the wire (a) Present Study (b) Lami et al. [11]

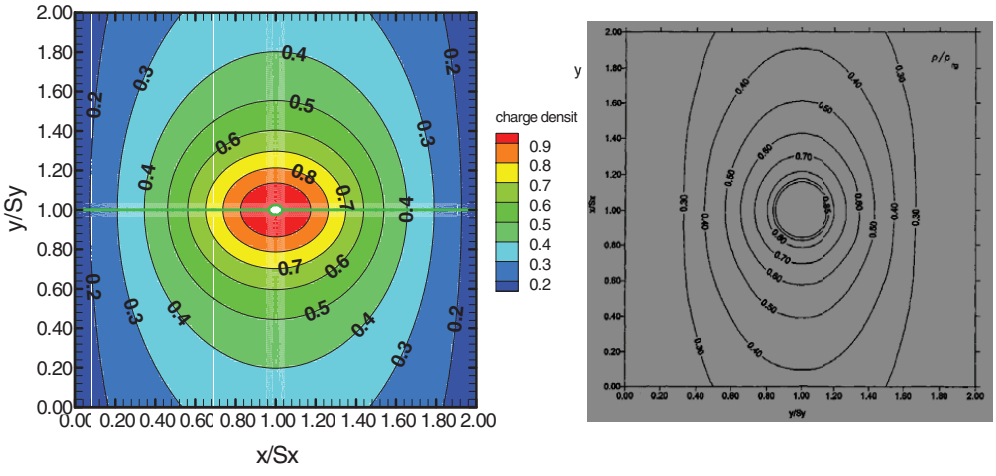

(a) Normalized spatial charge density – Present study

(b) Normalized charge density – Lami et a

Figure 10: Normalized spatial charge density distribution–charge density is normalized using the charge density at the wire (a) Present Study (b) Lami et al. [11]

expected the flow field and the concentration field vary with respect to the inlet gas velocities and the particle sizes. The numerical analysis is conducted for two particle sizes (1 µm and 10 µm) and for three inlet gas velocities (1.4, 4.5 and 5.6 m/s). It is seen from the results obtained that, for finer particles the removal efficiency of the wESP decreases drastically. The larger the particle the more easily it gets electrostatically precipitated. The results

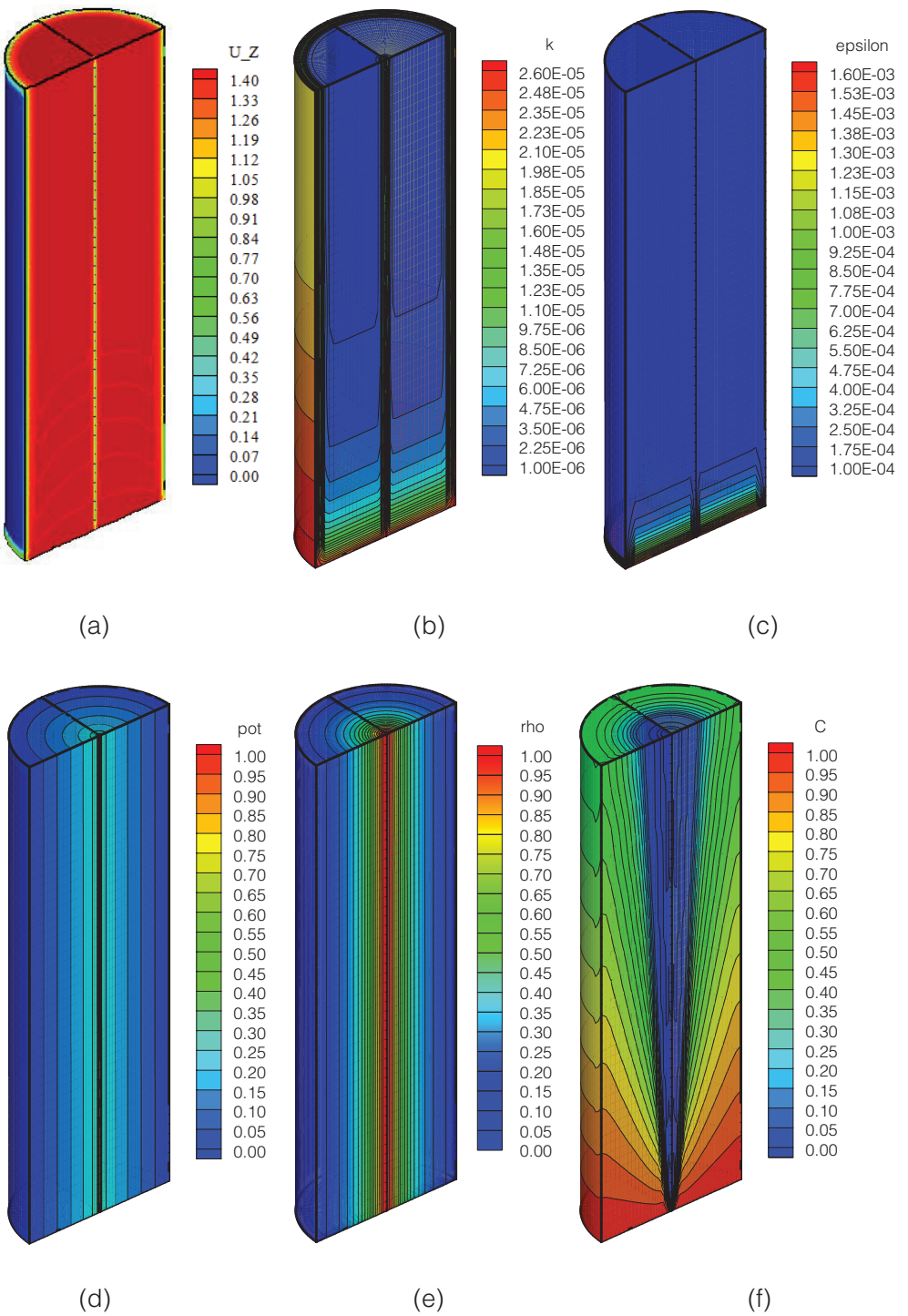

Figure 11: Contours of (a) z-velocity in m/s (b) turbulent kinetic energy in m^2/s^2 (c) turbulent dissipation rate m^2/s^3 (d) normalized electric potential (e) normalized space charge density (f) normalized concentration in one half of the wESP for an inlet gas velocity of 1.4 m/s and a particle size of 1 μm

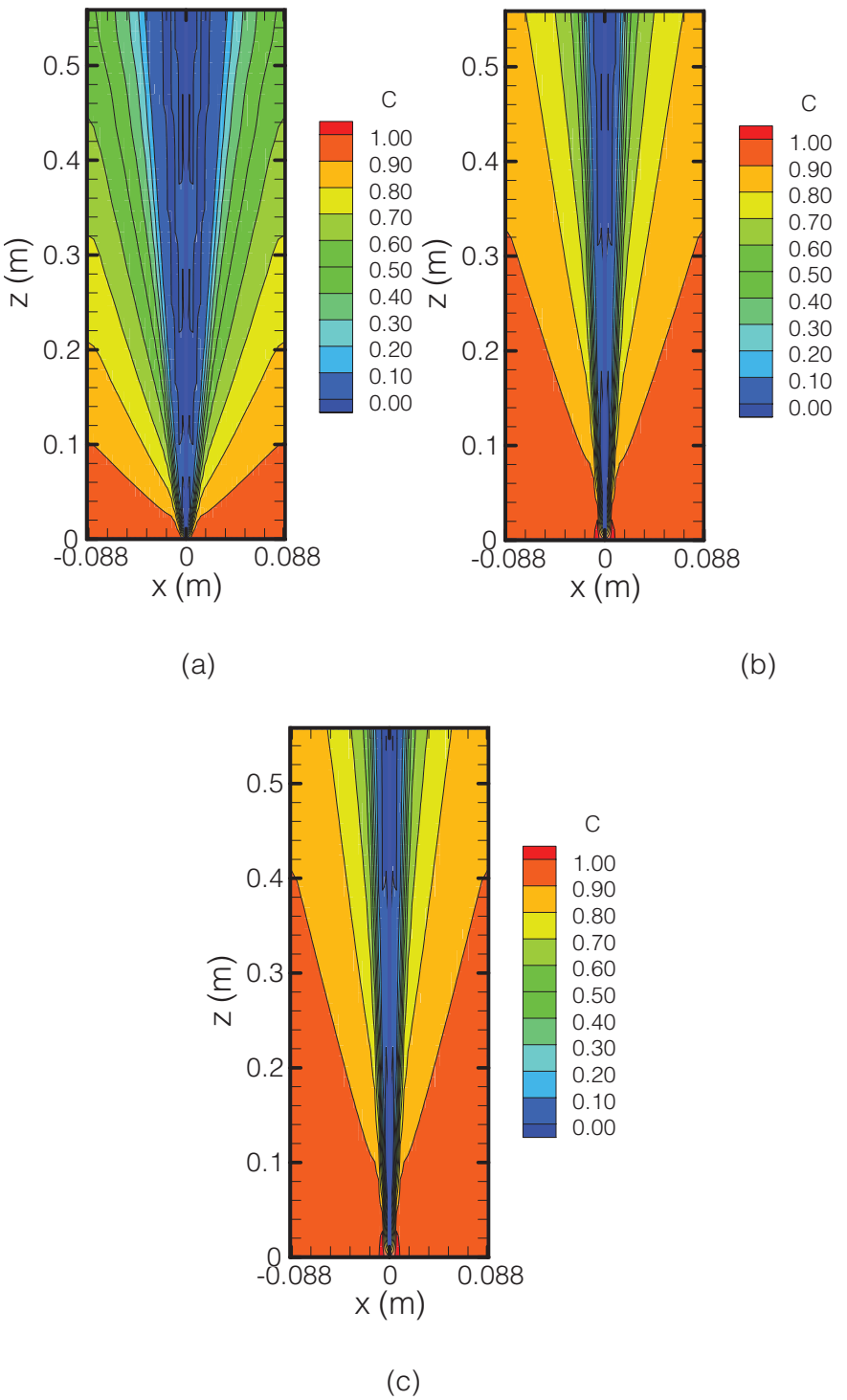

Figure 12: Normalized concentration distribution for a particle size of 1 μm at saturation charge for an inlet gas velocity of (a) 1.4 m/s, (b) 4.5 m/s and (c) 5.6 m/s.

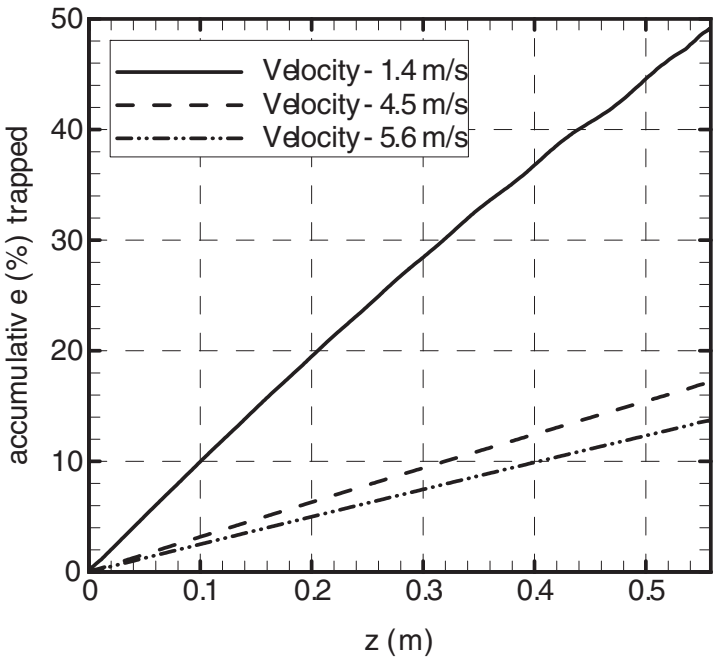

Figure 13: Collection efficiency of wESP for various inlet gas velocities for particles of 1 μm diameter at saturation charge.

presented for a particle size of 1 μm and 10 μm in Figs. 12 and 14 show that the removal efficiency is maximum for larger particles (10 μm) as compared to smaller sized particles (1 μm). The larger the particle the more the number of charges that gets deposited on it and thereby the particle experiences a higher electrostatic force. The removal efficiency is very low for sub micron sized particles as only a fraction of the particles present might assume a charge. For particles below 100 nm the number of units of charge acquired is quite less and thereby a longer wESP is recommended. The percentage of particles trapped along the length of the wESP for the two particle sizes (1 μm and 10 μm) are plotted in Fig. 13 and 15. It can be seen from Fig. 13 that the maximum accumulative percentage of particles trapped for a particle size of 1 μm is 49% at the exit of the wESP, corresponding to an inlet gas velocity

Table 3: Comparison of the predicted efficiencies with the efficiencies calculated from Deutsch–Anderson equation

Inlet gas velocities (m/s)	**Efficiency predicted using Deutsch Anderson Eqn (%)**	**Efficiency - particles of 1 μm diameter**		**Efficiency - particles of 10 μm diameter**	
		Saturation charge	**Half the saturation charge**	**Saturation charge**	**Half the saturation charge**
1.4	93.24	49	26.5	100	100
4.5	75.26	17	9	96	62
5.6	70.91	13.5	7	85	52

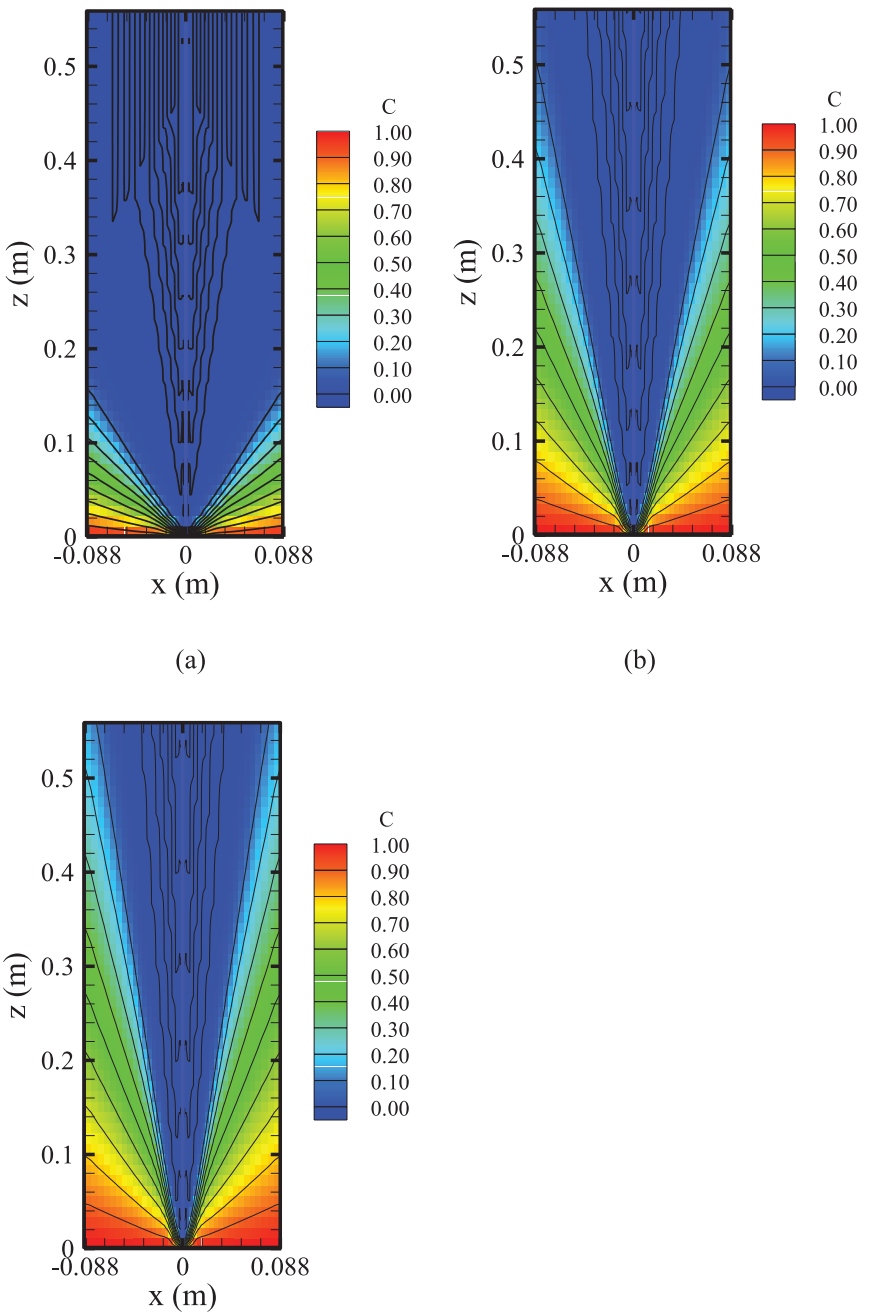

Figure 14: Normalized concentration distribution for a particle size of 10 μm at saturation charge for an inlet gas velocity of (a) 1.4 m/s, (b) 4.5 m/s and (c) 5.6 m/s.

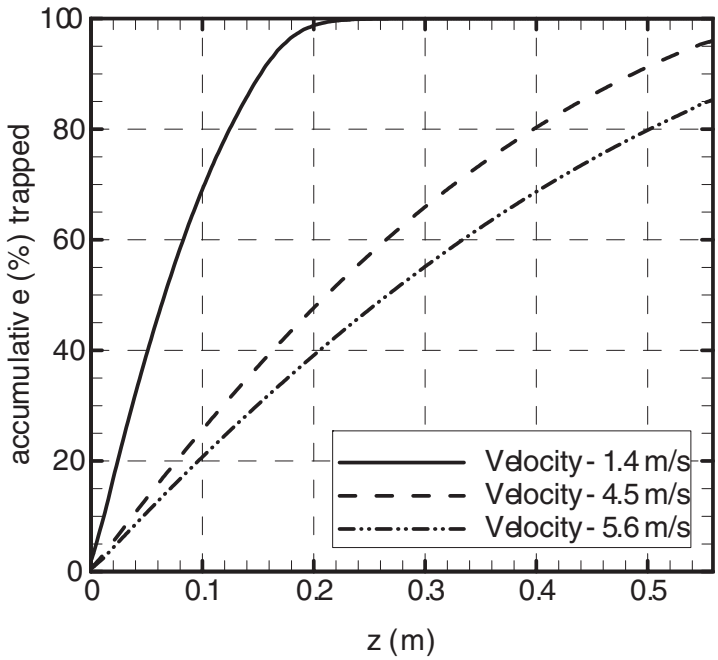

Figure 15: Collection efficiency of wESP for various inlet gas velocities for particles of 10 μm diameter at saturation charge

of 1.4 m/s. whereas, for a particle size of 10 μm the collection/removal efficiency is quite high and all the particles get electrostatically precipitated within a length of 0.25 m. From Table 3 one could infer that the collection/removal efficiency predicted for larger particles in the present study are closer to those predicted by Deutsch-Anderson equation. For smaller/finer particles the values of efficiencies predicted by Deutsch-Anderson equation can be totally misleading.

4.4. EFFECT OF NUMBER OF CHARGES ACQUIRED BY PARTICLES ON THE REMOVAL EFFICIENCY OF WESP

Figs. 16 and 18 present the contours of concentration at the symmetry plane (ZX plane) for a particle size of 1 μm and 10 μm respectively. The results presented in Figs. 16 and 18 are by considering that only half the maximum number of charges gets deposited on the particles. It is seen from Figs. 17 and 19 that the particle collection/removal efficiency is almost halved. From Fig. 12 and 16 it can be seen that the removal efficiency of the wESP for an inlet gas velocity of 1.4 m/s is 49% (if the particles acquire saturation charge) and if the particles acquire only half the maximum number of charge the efficiency is brought down to 26.5%. Hence, from the present investigation one could conclude that the removal/collection efficiency is directly proportional to the number of charges that the particles acquire.

4.5. EFFECT OF THE INLET GAS VELOCITY ON THE REMOVAL EFFICIENCY OF WESP

It is clearly evident from Figs 12–19 that the removal efficiency is higher when the inlet gas velocity is low. There exists an inverse proportionality between the inlet gas velocity and the removal/collection efficiency. A lower inlet gas velocity means that the particles have a

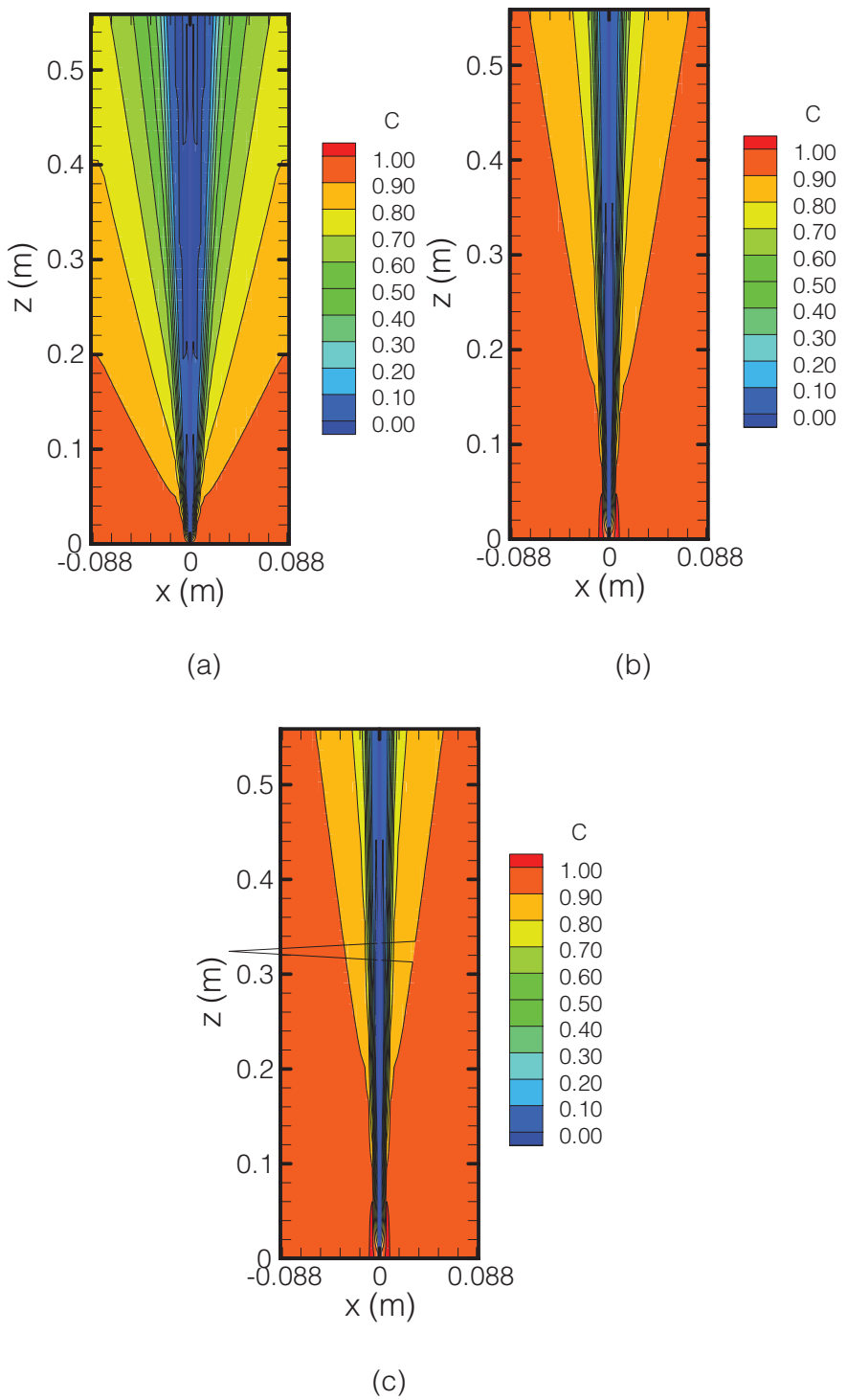

Figure 16: Normalized concentration distribution for a particle size of 1 μm at half the saturation charge for an inlet gas velocity of (a) 1.4 m/s, (b) 4.5 m/s and (c) 5.6 m/s.

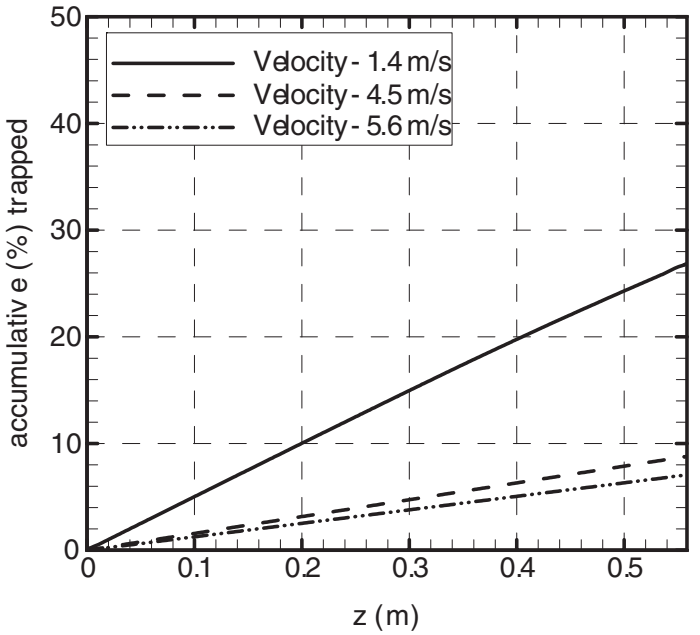

Figure 17 Collection efficiency of wESP for various inlet gas velocities for particles of 1 μm diameter at half the saturation charge

longer residence time and hence may get easily precipitated. By reducing the inlet gas velocity smaller particles may also be effectively captured for the same length of wESP. It can be seen from Fig. 13 that for a three times increase in the inlet gas velocity (i.e., from 1.4 m/s to 4.5 m/s) the removal efficiency for 1 μm particle is decreased from 49.5% to 17%. Similarly for a particle size of 10 μm the efficicency decreases from 100% to 96%. Table 3 shows the reduction in efficiency with change in inlet gas velocities and the number of charges acquired by the particles.

5. CONCLUSIONS

A modified drift flux model for predicting the collection efficiency of a tubular wESP has been used in the present study. The modified drift flux model can be used to predict the dispersion and removal of both fine (< 2 μm) and coarse mode particles (> 2 μm). The results presented for a particle size of 1 μm and 10 μm reveals that the larger the size of the particle the more easily it gets electrostatically precipitated. This behavior of larger sized particles is due to the number of charges that gets deposited on the surface of such particles. The investigation for various inlet gas velocities shows that there exists an inverse proportionality between the inlet gas velocities and the efficiency of electrostatic precipitation. From the present analysis it can be concluded that the efficiency of electrostatic precipitation increases with (i) an increase in particle size (ii) an increase in the number of units of charge on the particle (iii) and a decrease in inlet gas velocity.

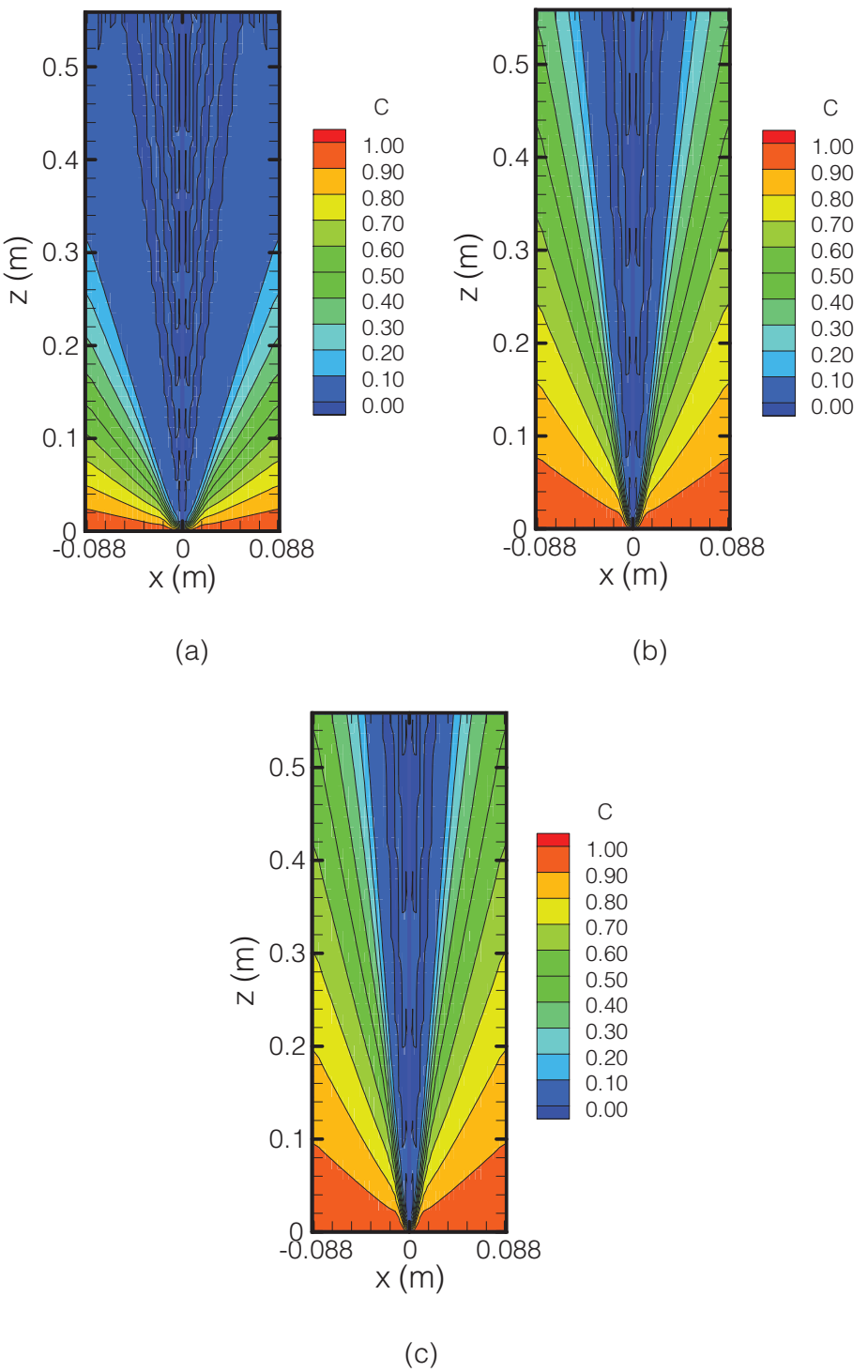

Figure 18: Normalized concentration distribution for a particle size of 10 μm at half the saturation charge for an inlet gas velocity of (a) 1.4 m/s, (b) 4.5 m/s and (c) 5.6 m/s.

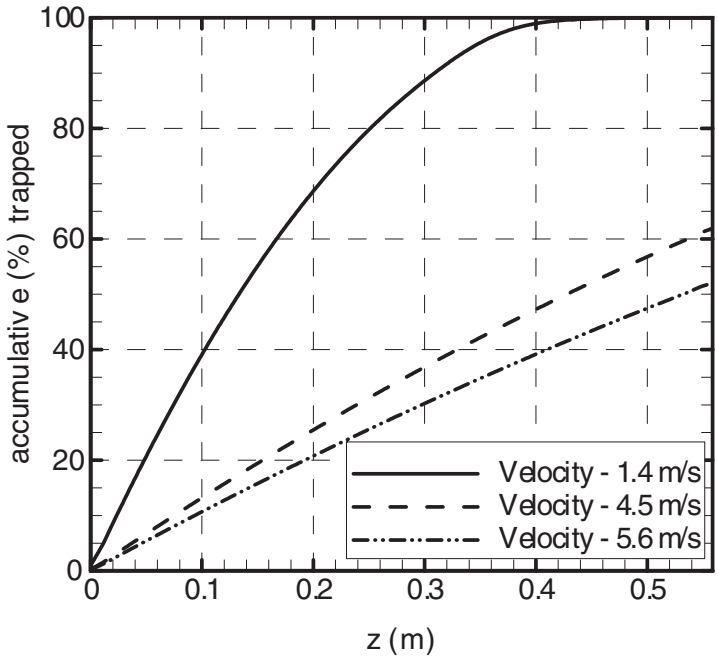

Figure 19: Collection efficiency of wESP for various inlet gas velocities for particles of 10 μm diameter at half the saturation charge.

NOMENCLATURE

b_I	ionic mobility = 23 × 10^{-4}, [m^2/V/s]
C_c	Cunningham correction factor
$\bar{C}_i$	mean thermal speed of ions = 2.43 × 10^{22}, [m/s]
C_0	particle number concentration at inlet, [#/m^3]
$\overline{C^\alpha}$	particle number concentration [#/m^3]
d_p	diameter of particles, m
D^∞	particle/Brownian diffusivity, [m^2/s]
D_t^α	turbulent diffusivity, [m^2/s]
e	electronic unit charge = 1.63 × 10^{-19}, [C]
E_j	electric field strength, [V/m]
i	coordinate index
j	coordinate index
k	turbulent kinetic energy, [m^2/s^2]
k_β	Boltzmann constant =1.38 × 10^{-23}, [J/K]
n_{field}	number of charges by field charging
n_{diff}	number of charges by diffusion charging
$\bar{p}$	pressure, [Pa]
q_p	charge of a single particle, [C]

Sc_t	turbulent Schmidt number
t	time, [s]
T	temperature, [K]
$\overline{u}_j$	velocity, [m/s]
u_j^t	terminal velocity, [m/s]
w_e	electrical migration velocity, [m/s]
x_i, x_j	position, [m]

Greek symbols

α	pollutant species
δ_{ij}	Kronecker delta
ε	turbulent dissipation rate, [m^2/s^3]
ε_0	dielectric permittivity of air = 8.859×10^{-12}, [As/V/m]
φ	electric potential, [V]
λ	mean free path of gas, [m]
μ	dynamic viscosity of gas, [kg/m/s]
μ_p	dielectric particle mobility, [As^2/kg]
μ_t	turbulent dynamic viscosity, [kg/m/s]
ρ	density, [kg/m^3]
$\rho_{el,I}$	ionic space charge density, [As/m^3 or C/m^3]
$\rho_{el,P}$	particulate space charge density, [As/m^3 or C/m^3]

REFERENCES

[1] Surati HS, Beltran MR, Raigorodsky. Tubular electrostatic precipitators of two-stage design. Environmental International 1981; **6** 239–244.

[2] Saiyasitpanich P, Keener TC, Khang SJ, Lu M. Removal of diesel particulate matter (DPM) in a tubular wet electrostatic precipitator. Journal of Electrostatics 2007; **65** 618–624.

[3] Bedmutha RJ, Ferrante L, Briens C, Berruti F, Inculet I. Single and two-stage electrostatic demisters for biomass pyrolysis application. Chemical Engineering and Processing: Process Intensification 2009; **48** 1112–1120.

[4] Jaworek A, Krupa A, Czech T. Modern electrostatic devices and methods for exhaust gas cleaning: A brief review. Journal of Electrostatics 2007; **65** 133–155.

[5] Soldati A. On the effects of electrohydrodynamic flows and turbulence on aerosol transport and collection in wire-plate electrostatic precipitators. Journal of Aerosol Science 2000; **31** 292–305.

[6] Ahmadi G. Modelling and computation of nanoparticles in fluid flows. Von Karman Lecture Series. RTO–AVT–VKI Lecture Series 2009.

[7] Xiangrong Z, Lianze W, Keqin Z. An analysis of a wire-plate electrostatic precipitator. Journal of Aerosol Science 2002; **33** 1595–1600.

[8] Schmid HJ, Vogel L. On the modelling of the particle dynamics in electro-hydrodynamic flow-fields: I. Comparison of Eulerian and Lagrangian modelling approach. Powder Technology 2003;135–136:118–135.

[9] He C, Ahmadi G. Particle deposition in a nearly developed turbulent duct flow with electrophoresis. Journal of Aerosol Science 1999; **30** 739–758.

[10] Penney GW, Matick RE. Potentials in D-C corona fields. Transactions of the American Institute of Electrical Engineers 1960; **79** 91–99.

[11] Lami E, Mattachini F, Sala R, Vigl H. A mathematical model of electrostatic field in wires-plate electrostatic precipitators. Journal of Electrostatics 1997; **39** 1–21.